Progress In Electromagnetics Research, PIER 37, 1–30, 2002

POLARIMETRIC EMISSION MODEL OF THE SEA AT MICROWAVE FREQUENCIES AND COMPARISON WITH MEASUREMENTS

K. St. Germain

Naval Research Laboratory
Washington, D.C. 20375, USA

G. A. Poe

Naval Research Laboratory
Monterey, CA 93943, USA

P. W. Gaiser

Naval Research Laboratory
Washington, D.C. 20375, USA

Abstract—A two-scale scattering model of the sea developed in terms of wind-generated stochastic processes of the surface-the elevation spectral density of the small-scale structure and the probability density of slopes of the large scale roughness-is combined with the Durden/Vesecky [1] wave height spectral model to analyze recent polarimetric measurements. Ad hoc parameter values are found for the wave model that allow the two-scale model to account for essentially all of the azimuthal features, amplitude and phase, appearing in all four Stokes parameters for the Jet Propulsion Laboratory (JPL) aircraft measurements at 19.35 and 37 GHz [2] and recent Naval Research Laboratory (NRL) aircraft measurements at 10.7 GHz. The excellent agreement provides support for the validation of the approximations of the two-scale model for the range of conditions encountered. The ad hoc parameters of the wave model are developed using the 19.35 and 37.0 GHz data and then tested with 10.7 GHz data. The two-scale model should be useful in studies dealing with simulations and retrievals of surface wind direction from satellite-based polarimetric measurements.

1 Introduction

2 Two-Scale Model

3 Sea Surface Wave Model

3.1 Model Selection

3.2 Model Parameters

4 10.7 GHz Polarimetric Radiometer System and Experiment Description

5 Data Processing and Measurement/Model Comparison

6 Simplified Polarimetric Model

7 Conclusions

Acknowledgment

References

1. INTRODUCTION

The ocean near-surface wind vector, which is critical for accurate storm forecasting, maritime planning and climatological studies, is strongly correlated with the magnitude and azimuthal behavior of ocean surface emission. The effect is apparent in both vertically and horizontally polarized channels, as well as in the third and fourth Stokes parameters [3]. Observations at 10.7, 19 and 37 GHz from an aircraft platform confirmed this behavior over a broad range of wind speeds (3 to 35 m/s) [4, 5]. The directional behavior of the brightness temperature takes the form of a sum of sinusoidal functions of relative wind direction (RWD), where RWD is defined as the angle between the azimuthal look direction of the sensor and the upwind direction. Two harmonics in RWD are present. Observations show that the directional behavior for the vertical and horizontal radiances is an even function (cosine) of the RWD while the directional behavior of the third and fourth Stokes parameters is an odd function (sine) of the RWD. Upwind and downwind are distinguished by the first harmonic while the second harmonic distinguishes between upwind/downwind and crosswind. The relative strengths of these harmonics depend on frequency, polarization, incidence angle, and wind speed. Specifically, observations have shown that the upwind-downwind asymmetries increase with increasing wind speed and incidence angle; the upwind-crosswind behavior is more dependent on polarization and incidence angle [5].

The potential of polarimetric microwave radiometry to measure the ocean surface wind vector has led to a significant amount of research, both in terms of observations and modeling. Wentz [6] analyzed SSM/I data and in situ measurements and derived a wind directional dependence for vertical and horizontal polarization at 19 and 37 GHz. More recently, this analysis was expanded to include additional buoys and the TRMM Microwave Imager (TMI) [7]. The new analysis used independent sources for ocean surface and atmosphere retrievals to decouple these two regimes. As a result, Meissner and Wentz conclude that the strength of the vertical and horizontal wind directional signals are significantly smaller than found in Wentz's earlier work [6], with virtually no signal for wind speeds less than 5 m/s. Others have also investigated the azimuthal dependence of the ocean surface emissivity using SSM/I and aircraft radiometer data. Chang and Li [8] used a limited set of SSM/I data and *in situ* measurements to develop a neural network algorithm to retrieve wind speed and wind direction with 180° ambiguity. By removing the wind direction effect on the measured brightness temperatures, they achieved wind speed retrieval accuracy of approximately 1 m/s, which is a significant improvement over the performance with no wind direction. Wick et al. [9] compared SSM/I data with wind directions from buoys and the ERS-1 and ERS-2 scatterometers. They confirmed the presence of wind direction dependence in the SSM/I data at 19, 37 and 85 GHz. They also noted no significant change in the wind direction signal for stable and unstable atmospheric conditions. Piepmeier and Gasiewski [10] reconfirmed the presence of the wind direction signal at 10, 19 and 37 GHz with a conically scanning airborne system. They used their data to develop a maximum-likelihood estimator retrieval algorithm to estimate wind direction over a narrow swath in the Labrador Sea. The results of these and other observation and modeling efforts has given impetus to the development of WindSat, a satellite-based polarimetric microwave radiometer for the demonstration of remote sensing of the ocean surface wind vector from space. The U.S. Navy and the National Polar-orbiting Operational Environmental Satellite System jointly sponsor WindSat.

To fully exploit the capabilities of the new microwave sensor technology and data, the Naval Research Laboratory has developed a two-scale electromagnetic scattering and emission model. The surface is modeled in terms of wind-generated stochastic processes of the surface — the elevation spectral density of the small-scale structure (i.e., capillary and short gravity waves) and the probability density of slopes of the large-scale roughness (i.e., gravity waves).

Herein we discuss the development of the polarimetric emission model by comparing calculations of the two-scale model with aircraft-based polarimetric measurements. In Section 2 we provide a brief overview of the two-scale model framework. In Section III we present comparisons of the two-scale model using the Durden/Vesecky wave model and derive a set of ad hoc parameters to fit aircraft polarimetric observations at 19 and 37 GHz [2] while maintaining consistency with the sensitivity of horizontal brightness temperature to windspeed [11]. A description of the NRL 10.7 GHz polarimetric radiometer is presented in Section 4 and followed in Section 5 with comparisons of recent 10.7 GHz aircraft measurements of the third and fourth Stokes parameters, which serve as an independent check on the validity of the model. Finally, a first-order model of the polarimetric information contained in the surface emissivity and scattered sky temperature is presented in Section 6.

2. TWO-SCALE MODEL

One of the first theoretical studies of the microwave radiometric emission and scattering of the sea surface by wind-driven waves [12] treated the sea as a normally distributed surface satisfying the Kirchhoff approximation (i.e., the mean wave height is much greater than the electromagnetic wavelength of interest.) Using the empirical Gaussian slope distributions of Cox and Munk [13], Stogryn predicted a significant sensitivity of the up-welling horizontally polarized brightness temperatures to ocean wind speed at 19.4 GHz, a small up-wind/cross-wind dependence and an invariant vertical polarization in the vicinity of 50° incidence angle. Attempts to verify the model predictions were undertaken by Hollinger [11, 14] at 1.41, 8,36 and 19.4 GHz using radiometric measurements from the Argus Island tower. Excluding patches of foam, Hollinger showed that Stogryn's geometric optics model provided qualitative agreement with the observed angular and wind speed behavior although it underestimated the wind speed sensitivity of the horizontal polarization at small incidence angles and failed to account for frequency dependence of the wind speed sensitivity. The short-comings of the geometric optics model were not altogether surprising in view of the fact that the Kirchhoff approximation is expected to be valid only for surfaces whose slopes are not too great and whose radii of curvature are large compared to the electromagnetic wavelength. This condition is met by large gravity waves but not satisfied by small ripples or capillary waves at microwave frequencies. In addition, as noted by Hollinger the only frequency dependence of Stogryn's model occurs in the dielectric constant of the

sea and primarily affects the absolute level.

Extending the Semyonev two-scale scattering theory [15], Wu and Fung [16] and Wentz [17] developed surface emission models to include the effects of small-scale roughness. In these models the ocean's surface was approximated by a random surface whose roughness scale is small compared with the electromagnetic wavelength (e.g., capillary waves) that resides on top of the large gravity waves characterized by their distribution of slopes. The resulting composite wave model provided considerably better agreement with Hollinger's observations thus verifying the importance of small-scale scattering effects. However, since the wave height spectrum of the small-scale roughness was assumed to be isotropic, wind direction dependencies of the vertical and horizontal brightness temperatures were not considered.

The scattering effects of anisotropic short-gravity and capillary waves on microwave ocean emissions, including all Stokes parameters, were investigated recently by Yueh, et al. [3, 18]. Like earlier two scale composite modeling, Yueh analyzed the scattering from the small scale roughness by means of small perturbation theory while the effects of the large scale structure was treated by geometric optics. Modifying the small scale wave spectrum of Durden and Vesecky [1] in conjunction with the Cox and Munk [13] large scale slope distribution, Yueh [2] obtained reasonably good agreement between the modeled polarimetric emission components of the Stokes brightness temperatures and aircraft observations at 19 and 37 GHz as a function of wind direction. The modifications of the elevation spectrum involved doubling the spectral amplitude and expansion of the hydrodynamic modulation process. In addition, Yueh employed a simple sea foam model, which affected only azimuthally averaged vertically and horizontally polarized emission components.

Herein, we continue to examine the applicability of the two-scale scattering model to explain the observed polarimetric signatures. NRL has developed a two-scale scattering model similar to that of Yueh [2], with the exception that (1) the composite differential scattering coefficients for the "coherent" scattered energies are evaluated in closed form and (2) the incident sky radiation scattered by the surface is included. In addition, the effect of shadowing waves is included, which becomes important at large incidence angles. The development of the NRL two-scale model [19] parallels the excellent exposition of Stogryn [20] of the first two Stokes parameters. To focus on the role of scattering by waves, we have restricted our attention to the foam-free surface and a fully developed sea. Clearly the emission of sea foam should be included once the emission and scattering properties are better understood. However, in spite of these and other deficiencies,

the two-scale model in concert with a suitable set of parameters reported herein for the Durden/Vesecky wave spectral model provides very good agreement with observations, suggesting that foam may play a secondary role in accounting for the wind direction signature.

3. SEA SURFACE WAVE MODEL

3.1. Model Selection

Assuming an elevation spectrum of the sea, W, may be established for all scales of roughness, it is common practice to approximate the small scale spectra, W_s, with a simple replication of W above a transition or cut-off wavenumber k_d

$$W_s(k,\phi) = \begin{cases} W(k,\phi), & k > k_d \\ 0, & k < k_d \end{cases} \tag{1}$$

and the large scale spectra W_l by

$$W_l(k,\phi) = \begin{cases} 0, & k > k_d \\ W(k,\phi), & k < k_d \end{cases} \tag{2}$$

(At some risk of notational confusion we will follow convention and use (k,φ) to denote the polar-coordinates of the wavenumbers in the up- and cross-wind directions associated with the rectangular coordinates (w_x, w_y) with the up-wind direction defined by $\varphi = 0$. The electromagnetic wavenumber of interest will now be identified by k_0.) We also assume that W_s is normalized so that the variance of the small scale wave height $\langle f^2 \rangle$ is given by

$$\left\langle f^2 \right\rangle = \int_0^{2\pi} d\phi \int_0^{\infty} dk\, k W_s(k,\phi) \tag{3}$$

The classic observations of Cox and Munk [13] show that for a clean sea surface the probability density of slopes for all scales of roughness is well-approximated by a skewed Gaussian distribution with principal axes in the up- and cross-wind directions. Furthermore, their measurements of an oil-covered surface indicate that the oil slick smoothed-out the capillary waves, leaving only waves greater than 30 cm and eliminated the up-wind skewness of the distribution. Since we are interested in the probability density of the large-scale waves we may neglect the skewness and characterize the density of slopes by a zero-mean bi-variate Gaussian distribution with variances of slopes

(σ_u^2, σ_c^2) for the principal axes computed on the basis of (2)

$$\begin{aligned} \sigma_u^2 &= \int_0^{2\pi} d\phi \cos^2\phi \int_0^\infty dk\, k^3 W_l(k,\phi) \\ \sigma_c^2 &= \int_0^{2\pi} d\phi \sin^2\phi \int_0^\infty dk\, k^3 W_l(k,\phi) \end{aligned} \tag{4}$$

From the point of view of oceanography the above procedure of constructing W_s and W_l appears to be a gross over-simplification, especially in the vicinity of k_d. However, the degree of validity of (1) and (2) for microwave polarimetry must, of course, be judged on the basis of the final comparisons of measurements and the two-scale model. The selection of k_d is somewhat arbitrary although k_d must satisfy the approximations of the two-scale model. First, k_d must be sufficiently large so that the ratio of the rms height of the small scale structure to the electromagnetic wavelength is much less than unity. Second, k_d must be sufficiently small compared with the electromagnetic wavenumber k_0 so that the Kirchhoff approximation remains valid for the large scale structure. As shown by Yueh [2] values of k_0/k_d can be found that allows satisfaction of both conditions with typical values lying in the range of 2 to 5 [21].

The directional dependence of W_s may be analyzed by expressing the total wave spectrum W in terms of an omni-directional spectrum $S(k)$ and a so-called "spreading" function $\Phi(k,\varphi)$

$$W(k,\phi) = k^{-1} S(k) \Phi(k,\phi) \tag{5}$$

with Φ satisfying the normalization

$$\int_0^{2\pi} d\phi \Phi(k,\phi) = 1$$

for each k.

To evaluate the two-scale emission model we have selected the wave height spectral model of Durden and Vesecky [1]. Durden and Vesecky employ the semi-empirical formulation of Fung and Lee [22] with a modification to the high-frequency component of the omni-directional spectrum but retain Fung and Lee's spreading function, which may be expressed as

$$\Phi(k,\phi) = \frac{1}{2\pi}[1 + \Delta(k)\cos 2\phi] \tag{6}$$

where

$$\Delta(k) = \left(\frac{1-R}{1+R}\right)\left(\frac{2}{1-D}\right)\left[1 - e^{-s_0 k^2}\right] \tag{7}$$

and R is the ratio of the variances of the cross-wind to up-wind slopes for the complete wave spectrum W. Fung and Lee compute R on the basis of the linear regression results of Cox and Munk [13] for a clean sea surface

$$R = \frac{3.0 + 1.92U_{12.5}}{3.16U_{12.5}} \tag{8}$$

where $U_{12.5}$ is the wind speed (m/s) at a height of 12.5 m. D is given by

$$D = \frac{\int_0^\infty dk\, k^2 S(k) e^{-s_0 k^2}}{\int_0^\infty dk\, k^2 S(k)} \tag{9}$$

with coefficient s_0 selected on the basis of matching radar backscatter model to measurements at 13.9 GHz. Fung and Lee propose $s_0 = 1.5 \cdot 10^{-4}\,\mathrm{m}^2$ but recommend that both R and s_0 be re-evaluated when more data become available.

To account for up-wind/down-wind asymmetry absent in the spreading function, Durden/Vesecky incorporate hydrodynamic modulation of the small waves by the large scale waves. The modulation process is approximated by a simple weighting of the small scale spectrum by a linear function of the large scale slope in the up-wind direction to emphasize the small scale spectrum on the down-wind side of the large scale waves. Following this approach, Yueh [2] introduced a slight modification to limit the weighting when the large scale slope in the up-wind direction ξ_u exceeds 1.25 times the standard deviation of the up-wind slope σ_u

$$h(\xi_u) = \begin{cases} 1 + m\,\mathrm{sgn}(\xi_u) & \text{where} \quad |\xi_u| > 1.25\sigma_u \\ 1 + \dfrac{m}{1.25}\left(\dfrac{\xi_u}{\sigma_u}\right) & \qquad\quad |\xi_u| \le 1.25\sigma_u \end{cases} \tag{10}$$

where m provides a measure of the degree of modulation. (sgn $(x) = 1$ when $x > 0$ and -1 when $x < 0$.) Yueh selected $m = 0.5$. In addition, Yueh recommended that the scalar multiplier of the total spectrum a_0 appearing in the Durden/Vesecky model be doubled to $a_0 = .008$. As noted by Yueh, the larger a_0 results in a total variance of slopes that is approximately 1.9 greater than that measured by Cox and Munk, but is in reasonable agreement with Donelan and Pierson [23]. We incorporate Yueh's parameters and henceforth refer to the Durden/Vesecky model with Yueh's modifications as the Durden/Vesecky/Yueh model.

The polarimetric brightness temperature measurements we have selected for comparison with the two-scale emission model are those

reported by Yueh [2] at 19.35 GHz for an ocean windspeed of 9 m/s (5 m) at a 55° earth incidence angle. We feel these data, taken under cloud-free conditions, are representative of microwave polarimetric signatures for all four Stokes parameters and, as such, provide a realistic test to assess the applicability of the above noted spectral models. Since the reflection and scattering of the incident sky brightness temperature are included in the two-scale model, we approximate the incident sky temperature by an azimuthally invariant form

$$T_{sky}(\theta) = \overline{T}_{air}\left(1 - e^{-\kappa \sec\theta}\right) \tag{11}$$

where θ is the earth incidence angle, κ is the zenith opacity and $\overline{T}_{air}$ is the effective air temperature. For these data we take the opacity to be 0.05 at 19.35 GHz which, for a cloud-free condition, corresponds to a water vapor mass (columnar) of 20 mm and is consistent with area and time of observations. Buoy measurements indicate a sea surface temperature of 285 K. We assume a surface salinity of 35‰ and approximate $\overline{T}_{air} = T_{air} - 11$ K. We have used a two-relaxation time Debye model for the complex dielectric constant of sea water [24].

3.2. Model Parameters

In an attempt to improve the comparisons between polarimetric measurements and the two-scale model computations we conducted an ad hoc sensitivity study of several parameters appearing in the Durden/Vesecky/Yueh spectra model. Model parameters selected include the coefficient s_0 (7), the ratio R of cross-wind to up-wind slope variances for the total spectrum (8), the degree of hydrodynamic modulation m (16), the scalar multiplier a_0 of the wave spectra and the ratio k_0/k_d. Note that m controls the up- to down-wind asymmetry while R influences the up- to cross-wind asymmetry. The ratio k_0/k_d and a_0 affect the magnitudes of the third and fourth Stokes parameters.

We have selected the measurement data set for the sensitivity study to contain the following: (A) aircraft polarimetric observations at both 19 and 37 GHz for cloud-free conditions with windspeed of $U_5 = 9$ m/s at 55° incidence angle (the fourth Stokes parameter was not measured at 37 GHz) Yueh [2]; (B) Argus Island tower measurements of Hollinger [11, 14] at 8.36 and 19.35 GHz of the average horizontally polarized sensitivity to windspeed at 55° incidence angle; (C) SSM/I 19.35 and 37 GHz vertical and horizontal polarimetric signatures derived by Wentz [6] for three windspeed regimes of $U_{19.5}$: 0–6, 6–10 and above 10 m/s. For (A) we have employed a zenith opacity of 0.06 at 19.35 GHz and 0.08 at 37.0 GHz, which are consistent with values estimated by Yueh [5], while for (B) we selected average

opacities of 0.075 (19.35 GHz) and 0.10 (37 GHz) and average sea temperature of 285 K and $\overline{T}_{air} = 274\,\mathrm{K}$. For (C) we used opacities of 0.075 (19.35 GHz) and 0.017 (8.36 GHz) with sea temperature of 291.5 K and $\overline{T}_{air} = 280.5\,\mathrm{K}$. Data (A)–(C) provide an important test of the range and acceptability of the model parameters. Brief discussions of the results of the sensitivity study follow.

First, for (A), the coefficient s_0, varied from 10^{-5} to 10^{-3}, had a relatively small impact on the third and fourth Stokes parameters at 19 and 37 GHz (e.g., less than 0.1 K). The impact on the vertical and horizontal polarimetric signatures was larger but tended to degrade the comparisons as s_0 departed significantly from $1.5 \cdot 10^{-4}\,\mathrm{m}^2$. We have therefore retained the value selected by Fung and Lee.

Second, for (A), noticeably better comparisons occurred for the third and fourth Stokes parameters when k_0/k_d was larger than the value 3.369 selected by Yueh. This result combined with the desire to comply with the two-scale model approximations led us to select $k_0/k_d = 5.0$, a value considered but not used by Yueh.

Third, for (A), selecting a_0 substantially above 0.008, e.g., 0.01–0.012, resulted in excessively large down-wind polarimetric amplitudes for the vertical and horizontal Stokes parameters as well as significant distortion of the third Stokes parameters in the vicinity of the down-wind direction. Consequently, we have retained the value $a_0 = 0.008$ selected by Yueh.

Fourth, for (A), we found that both m and R have significant impacts on the comparisons. As m was varied from 0.3 to 1.0 and R from 0.40 to 0.90 we found that the "best" over-all agreement was achieved with m and R lying in the vicinity of 0.75 and 0.65, respectively. Subsequent comparisons with (B), i.e., the azimuthal averaged sensitivity of the horizontal brightness temperature to windspeed at 55°, however showed that the two-scale model over-estimated the sensitivity to windspeed by a factor of 2. Hollinger [11] measured sensitivities of $0.60 \pm 0.12\,\mathrm{K/m/s}$ (8.36 GHz) and $1.06 \pm 0.16\,\mathrm{K/m/s}$ (19.35 GHz) at a 55° incidence angle for a platform height of 43.3 m. To address this discrepancy while keeping the near "optimum" values $m = 0.75$ and $R = 0.65$, we investigated the impact of reducing the large scale slope variances determined by (4). It was found that a 50% reduction brought the two-scale model windspeed sensitivities into agreement with Hollinger's. For example, the 19.35 GHz (up-wind, cross-wind) slope variances associated with a windspeed $U_5 = 9\,\mathrm{m/s}$ or $U_{43.3} = 11.0\,\mathrm{m/s}$ and $k_0/k_d = 5.0$ were reduced from (0.0251, 0.0238) to (0.0126, 0.0119). Interestingly the reduced variances are nearly the same as those observed by Cox and Munk for an oil-covered sea (0.0127, 0.0113). To maintain agreement

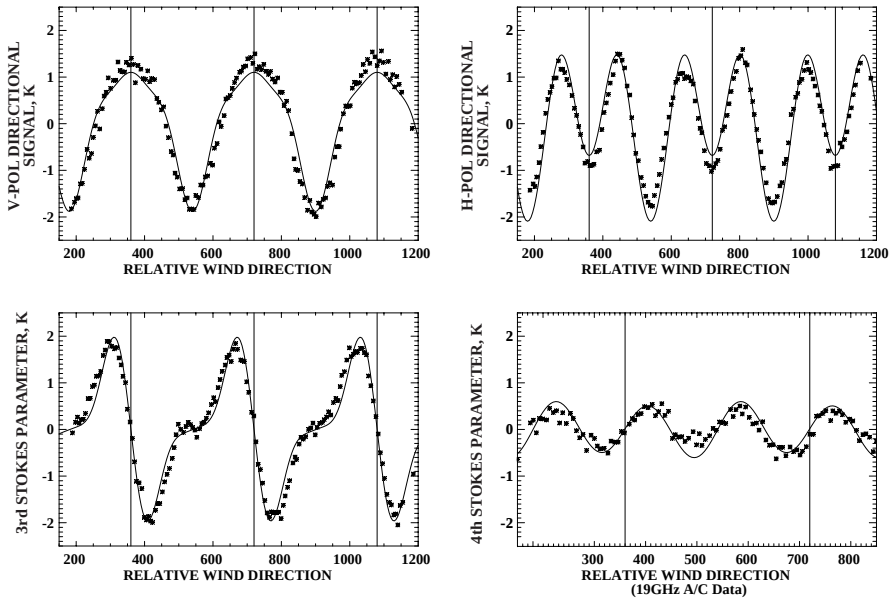

Figure 1. Comparisons of 37 GHz Aircraft Measurements (*) and DVY Model ($m = 0.75,\ R = 0.65;\ k_0/k_d = 5.0$) for $U_5 = 9\,\mathrm{m/s}$ and 55° Incidence Angle (Vertical Lines Identify Upwind Direction). The fourth Stokes parameter shown is at 19.35 GHz because the data were not available at 37 GHz.

with Hollinger's result, we shall henceforth reduce the large-scale slope variances of (4) by 50%. Apparently, a substantial portion of the large-scale waves does not contribute to the azimuthally-averaged sensitivity of the horizontal brightness temperature to windspeed.

Figures 1 and 2 present comparisons of the two-scale model and aircraft measurements (A) at 37 and 19.35 GHz for a windspeed $U_5 = 9\,\mathrm{m/s}$ and 55° incidence angle. The fourth Stokes parameter was not available at 37 GHz. The "optimized" spectral model parameters used: $s_0 = 1.5 \cdot 10^{-4}\,\mathrm{m}^2$, R = 0.65, m = 0.75 and $k_0/k_d = 5.0$ with a 50(4). These results demonstrate the ability of the two-scale model in conjunction with the Durden/Vesecky/Yueh spectral model to accurately describe the observed polarimetric signatures at 19 and 37 GHz. Excellent agreement occurs for all four Stokes parameters with the largest differences appearing in the down-wind direction for the horizontal polarizations at 19.35 GHz.

Possible windspeed dependence of the model parameters was investigated using data set (C). Wentz [6] derived a simple model

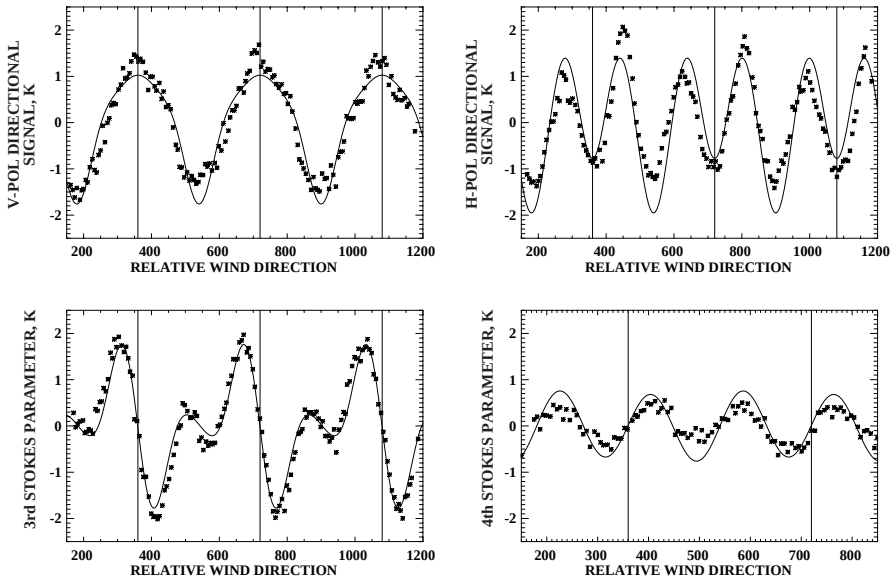

Figure 2. Comparisons of 19.35 GHz Aircraft Measurements (*) and DVY Model ($m = 0.75$, $R = 0.65$; $k_0/k_d = 5.0$) for $U_5 = 9\,\mathrm{m/s}$ and 55° Incidence Angle.

of the vertical and horizontal polarimetric signatures of the SSM/I data for three windspeed bins 1–6, 6–10 and above 10 m/s. To account for the averaging effects of the bins we have weighted the two-scale model computations within these bins by the distribution of windspeeds associated with the F-8 SSM/I matchups with NOAA buoy observations. We also restricted the windspeed range to 0.25–17 m/s, quantized in 0.5 m/s interval, with resulting average windspeeds of 4.1, 7.9 and 12.1 m/s for the respective bins.

Preliminary comparisons revealed that reasonably good agreement occurred for both vertical and horizontal polarizations for the 12.1 m/s bin but that the two-scale model significantly underestimated Wentz's model for the lowest windspeed bin. The source of the discrepancies was traced to the persistence of a relatively large up-wind/down-wind asymmetry in Wentz's results for the lower windspeeds, especially for the horizontal polarization. To address the situation we investigated the impact of allowing m to increase and R to decrease at the lower windspeeds. Figures 3 and 4 present comparisons when R is computed on the basis of

$$R(U_5) = \frac{0.25}{6} U_5 + 0.275 \tag{12}$$

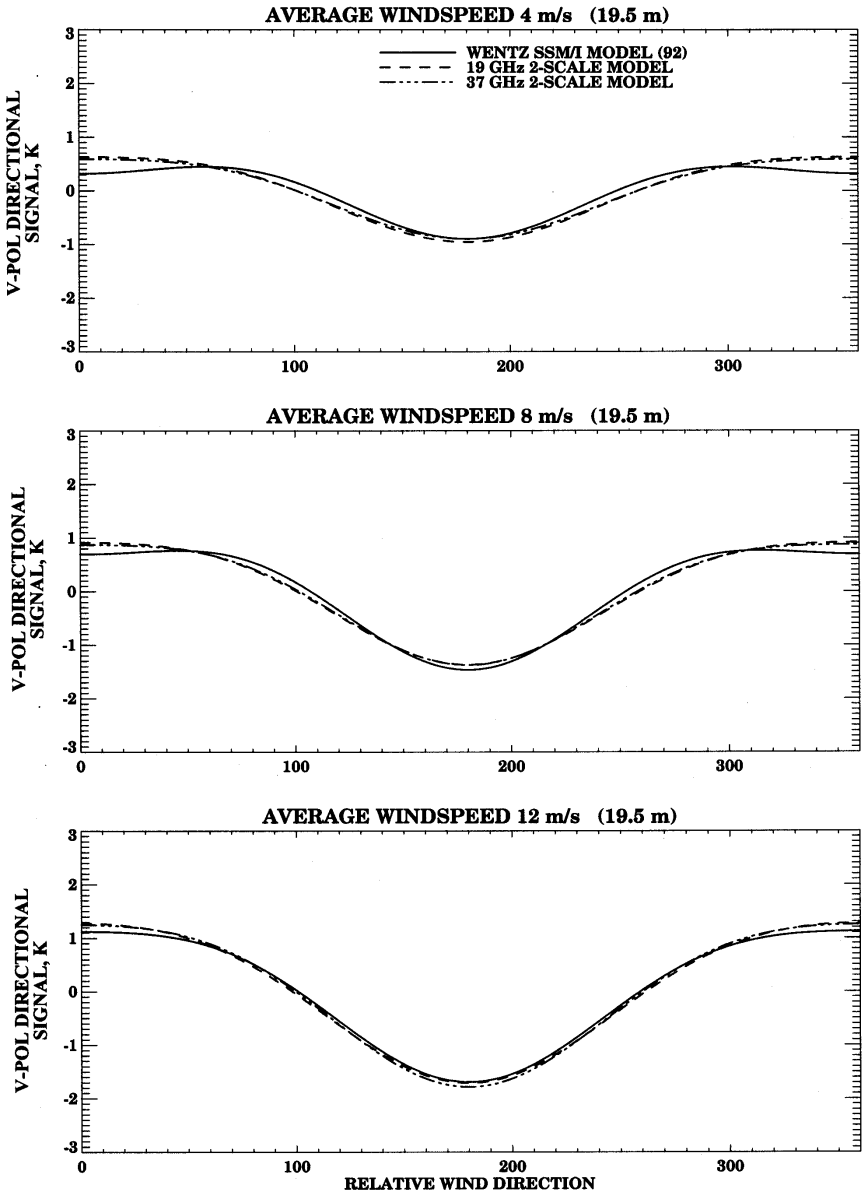

Figure 3. Comparisons of Wentz Polarimetric Model [6] and DVY Model (m and R Defined by (19) and (18) Respectively, $k_0/k_d = 5.0$) for Vertical Polarization.

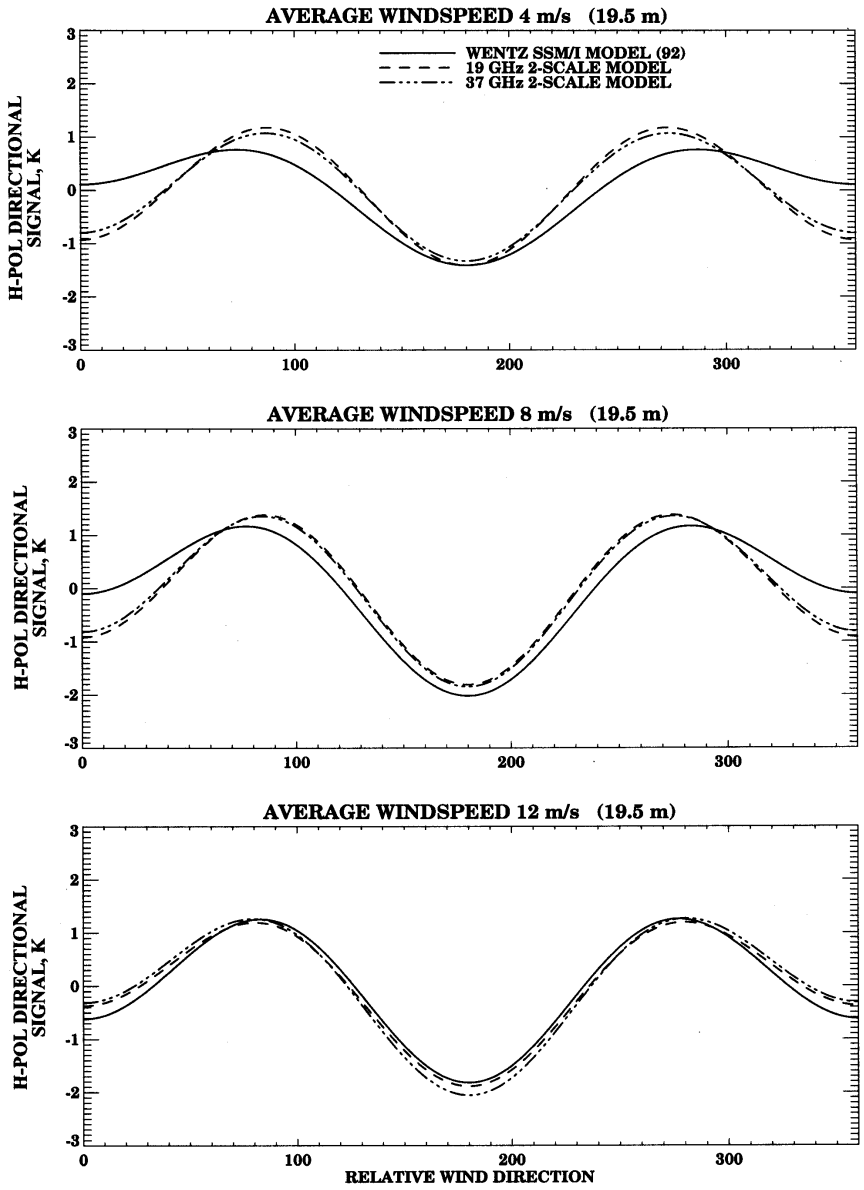

Figure 4. Comparisons of Wentz Polarimetric Model [6] and DVY Model (m and R Defined by (19) and (18) Respectively, $k_0/k_d = 5.0$) for Horizontal Polarization.

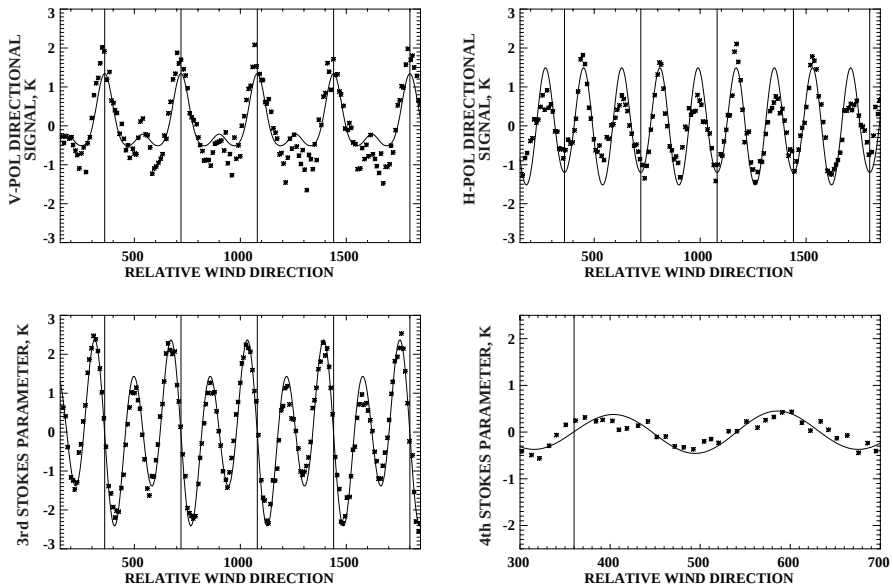

Figure 5. Comparisons of 19 GHz Aircraft Measurements (*) and DVY Model ($m = 0.75,\ R = 0.65;\ k_0/k_d = 5.0$) for $U_5 = 9\,\mathrm{m/s}$ and 45° Incidence Angle.

and m is taken to

$$m(U_5) = \begin{cases} 1.0 & U_5 \leq 6 \\ -\dfrac{0.25}{3}U_5 + 1.5 & 6 \leq U_5 \leq 9 \\ 0.75 & U_5 \geq 9 \end{cases} \tag{13}$$

where U_5 is the windspeed m/s at a 5 m height.

Very good agreement occurs for the vertical polarization for all three windspeed bins. Differences are typically less than 0.1–0.2 K and are consistent with the accuracy of Wentz's results. The agreement for the horizontal polarization is also good except for the region about the up-wind direction at the lower windspeeds. Apparently the model parameters (12) and (13) do not completely account for the large up-wind/down-wind asymmetry appearing in the horizontal polarization at the lower windspeeds. On the other hand, due to the relatively large scatter in the horizontal polarimetric signal (about 8 times larger than the vertical) it is possible that the accuracy of the Wentz model suffers at the lower windspeeds, especially near the up-wind direction. Clearly additional measurements are needed to resolve this issue. In

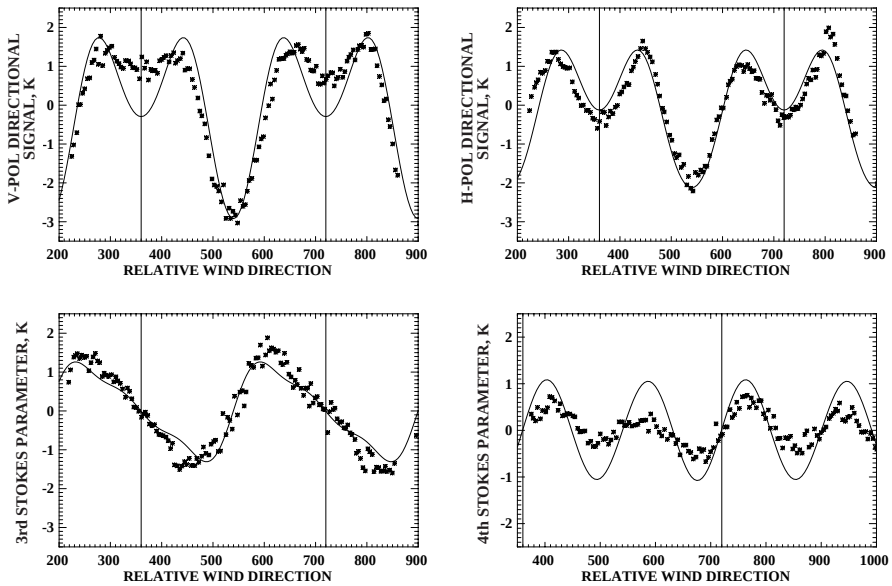

Figure 6. Comparisons of 19 GHz Aircraft Measurements (*) and DVY Model ($m = 0.75$, $R = 0.65$; $k_0/k_d = 5.0$) for $U_5 = 9\,\mathrm{m/s}$ and 65° Incidence Angle.

view of the good agreement for the vertical polarization, Figure 3, we retain the windspeed dependence of R and m defined by (12) and (13), realizing the discrepancy with Wentz's results at the lower windspeeds.

Finally, to assess the applicability of the model parameter for other incidence angles, Figures 5 and 6 present comparisons of the two-scale model with aircraft observations at 19.35 GHz for incidence angles of 45° and 65°, Yueh [2]. Again, excellent agreement occurs for all four Stokes parameters with the exception of the amplitude of the fourth Stokes and the vertical polarization in the up-wind direction at 65°.

4. 10.7 GHZ POLARIMETRIC RADIOMETER SYSTEM AND EXPERIMENT DESCRIPTION

The Naval Research Laboratory's 10.7 GHz polarimetric radiometer is depicted in Figure 7. The radiometer measures the two primary polarizations plus the third and fourth Stokes parameters via a polarization combining network similar to that described by Yueh et al. [25]. The antenna is a lens-corrected circular corrugated horn, followed by an orthomode transducer, which splits the incoming signal into

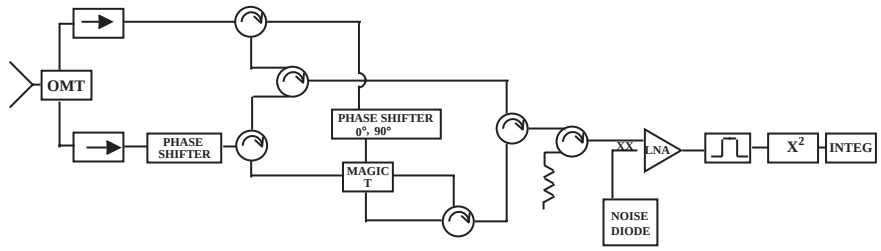

Figure 7. Block Diagram of the NRL 10.7 GHz polarimetric radiometer. The network of switches, phase shifters and Magic-Ts sequentially forms the +45, −45, left circular and right circular polarizations from the two primary polarizations, V and H.

vertical and horizontal polarizations. A network of ferrite switches then either sends the primary polarizations to the single receiver chain or sends both to a 180° hybrid (Magic-T) to form the ±45° polarizations. A switchable 90° phase shifter in the vertical arm of the Magic-T enables the formation of left- and right-circular polarizations. The switches and phase shifter are controlled by the data acquisition software, which drives them sequentially to measure six polarizations. The selected polarization is then amplified, filtered and detected in a noise-injecting Dicke radiometer. The performance parameters of the radiometer are shown in Table 1.

Ideally, the path loss in the vertical and horizontal chains should be balanced entering the Magic-T. Under these balanced conditions the third Stokes parameter T_U would be formed by simply taking the difference between the calibrated +45° and −45° polarizations and the fourth Stokes parameter would be formed from the difference of the left- and right-circular polarizations. The effect of imbalances between the chains is a coupling between the third and fourth Stokes parameters. Since the system is not ideal we measured the path loss and phase delay for each chain at both the 0° and 90° phase shifter settings. These data are used in the post-flight data processing to decouple the third and fourth Stoke's parameters.

A joint campaign was staged with Jet Propulsion Laboratory (JPL) out of the NASA Wallops Flight Facility aboard the NASA P-3B aircraft on November 18, 20, 21, and 22, 1996. JPL operated 19 GHz and 37 GHz polarimetric radiometers. The flights were centered on a series of NOAA buoys off of the mid-Atlantic coast. Of the four flights, only the flight on the last day represented a fully developed sea state. On Nov. 22, the winds at buoy 41001 (located at 34.5 N, 72.4 W) began to increase at 9:00am, and increased steadily to 15 m/s

Table 1. System performance specifications for the NRL 10.7 GHz polarimetric radiometer. Spatial resolution calculations assume nominal flight altitude of 25,000 ft. Radiometric stability refers to the calibration drift over a period of 5 hours, which is the typical flight duration. This is one component of the absolute accuracy.

Parameter		Performance
Beam width		8 degrees
Beam Efficiency		95%
Spatial Resolution	**EIA=45°**	1.5 Km by 2.1Km
	EIA=55°	1.9 Km by 3.3 Km
	EIA=65°	2.5 Km by 6.1 Km
Bandwidth		250 MHz
Noise Figure		3.64 dB
Integration time		100 ms
Nominal NEDT		0.11 Kelvin
Absolute Accuracy		±3 Kelvin
Radiometric Stability		±0.15 Kelvin

at 10:30am. The winds remained relatively constant until 4:30pm, when they began to decrease slightly.

The polarimeter mounted at a window port in the aircraft, viewing 15° below the horizon. Accordingly, with the aircraft engaged in a fixed bank ranging from 10°–30° the local earth incidence angle ranges between 65° and 45°. The variability of roll was usually less than 1.5°. Typically, three circles were made about the buoy at each incidence angle. Prior to and immediately following each set of turns, controlled rolls of the aircraft are executed to allow the radiometer to view the horizon and the sky. These maneuvers provide data for instrument calibration and aircraft attitude correction. Time, latitude, longitude, heading, ground speed, pressure altitude, pitch and roll were recorded once per second by the aircraft inertial navigation system (INS).

5. DATA PROCESSING AND MEASUREMENT/MODEL COMPARISON

The radiometric measurements are processed in stages to calibrate the radiometer counts and compensate for the effects of minor variations in the aircraft pitch and roll, which introduce a rotation of the

polarization basis and vary the incidence angle.

In the first stage of data processing, the two internal calibration sources, a matched termination and a noise diode, provide the primary brightness temperature calibration. The noise diode effective brightness temperature is calibrated using external hot and cold loads prior to the flight. Data from the controlled rolls of the aircraft allow the radiometer to view the horizon and the sky, providing regular verification of the internal noise diode calibration source. Using these two sources for reference, internally monitored temperatures, and preflight path loss measurements, the radiometer counts are converted to raw radiance measurements for the six polarizations. The measured third and fourth Stokes parameters are formed by taking the difference of the plus- and minus-45 degree polarizations and the left- and right-circular polarizations respectively.

The second phase of data processing corrects for the coupling between the third and fourth Stokes parameters that is introduced by channel-to-channel gain and phase imbalances. Pre-flight and post-flight measurements of the gain and phase delay for each path establish the level of the cross coupling. We used these measurements to decouple the two signals. Because the instrument looks out the side of the aircraft, any variation in the aircraft pitch introduces a rotation of the polarization basis, which causes additional coupling between the primary polarizations and the third stokes parameter. INS measurements of the aircraft pitch are used to rotate the polarization basis back to an earth surface reference [25]. We verified that the fourth Stokes parameter was indifferent to rotation of the polarization basis, which should be the case when the correction for gain and phase imbalances has been made properly.

Finally, a correction is made for variations in the earth incidence angle caused by variations in the aircraft bank angle during the circle flights. During the roll maneuvers prior to and following the circles, the instrument sweeps through the earth incidence angles (EIA) of interest. These measurements are used to establish a functional relationship between the aircraft roll angle and the observed brightness temperature in the neighborhood of the EIA of interest. This relationship is then used to correct the radiometric measurements back to the desired EIA.

The absolute accuracy of the 10.7 GHz radiometer after these corrections is approximately ± 3 K with a stability of 0.1–0.2 K over the measurement period. Remaining biases in the T_U and T_V, due to residual calibration errors in T_{45}, T_{-45}, T_{lc} and T_{rc}, are removed by requiring that mean T_U and T_V over 360° of azimuth be zero.

We wish to compare the measurements at 10.7 GHz with those predicted by the two-scale model. Because the model is intended to

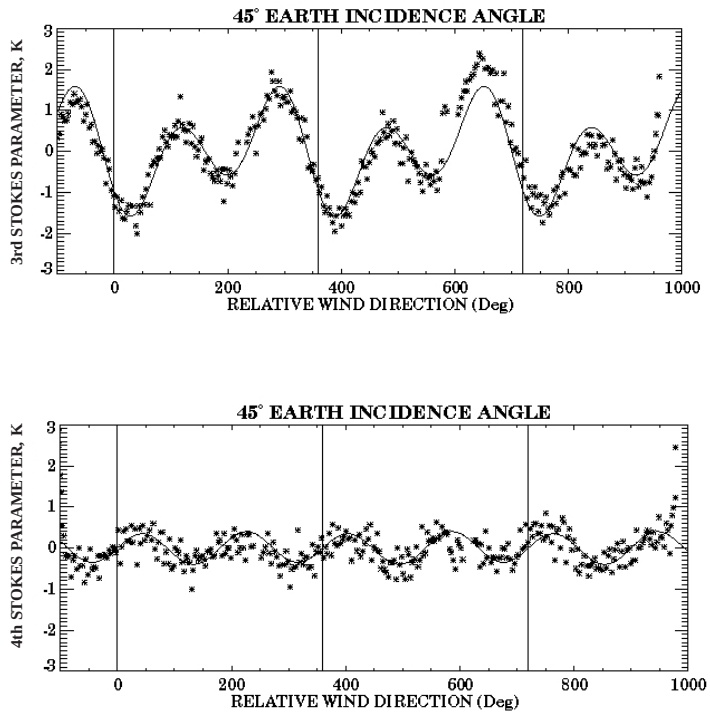

Figure 8. Comparisons of 10.7 GHz Aircraft Measurements (*) and DVY Model ($m = 0.75,\ R = 0.775;\ k_0/k_d = 5.0$) for $U_5 = 13\,\mathrm{m/s}$ and 45° Incidence Angle.

represent only fully developed sea states, we will limit the comparison to the data collected under steady state conditions, which occurred on November 22. On that day, we made three sets of measurements. For the first set, the winds were 15.2 m/s while for the second and third sets the winds were 13.6 m/s. The wind direction was steady, blowing from 329° throughout the day, with maximum recorded gusts of 19.1 m/s from 320. The significant wave height was 4.7 m, the surface air temperature was 13.7°C and the sea temperature was 22.2°C. The aircraft altitude was 26,000 feet with uniform, heavy cloud cover below and clear skies above. We have chosen a relatively large average zenith opacity of 0.03 for 10.7 GHz, consistent with heavy non-precipitating cloud cover.

Comparisons of the 10.7 GHz aircraft measurements at 13.6 m/s windspeed and the two-scale model calculations of the third and fourth

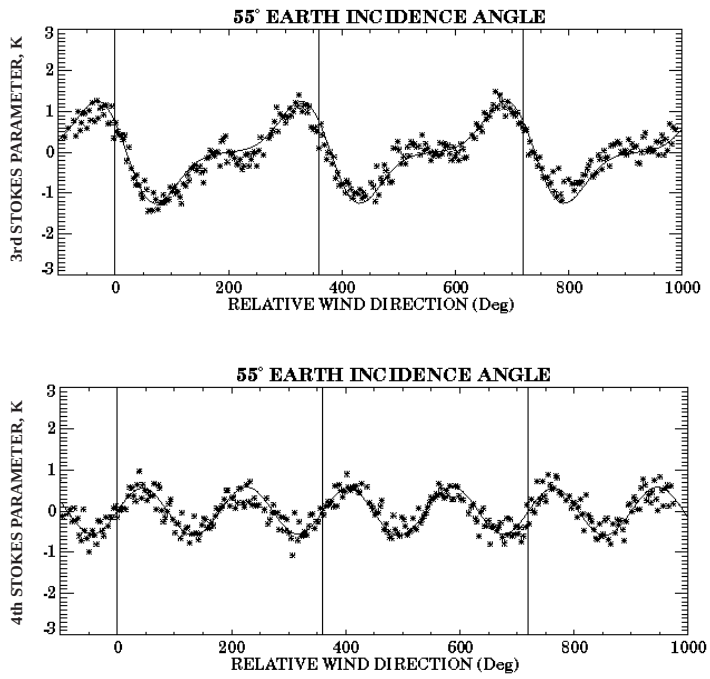

Figure 9. Comparisons of 10.7 GHz Aircraft Measurements (*) and DVY Model ($m = 0.75,\ R = 0.775;\ k_0/k_d = 5.0$) for $U_5 = 13\,\mathrm{m/s}$ and 55° Incidence Angle.

Stokes parameters are presented in Figures 8–10 for incidence angles of 45°, 55° and 65°. Excellent agreement occurs for all incidence angles with the largest difference appearing at 65° for the third Stokes parameter in the region about the up-wind direction. Unfortunately, due to the highly variable cloud cover over the flight path we were unable to make similar comparisons for the vertical and horizontal polarimetric signals. However, additional comparisons of the third and fourth Stokes parameters were possible for adverse weather conditions.

Comparison with measurements for a surface windspeed of 15 m/s (5 m), under heavier cloud conditions, are presented in Figures 11–13. (We selected an average zenith opacity of 0.05 for these comparisons.) Although the vertical and horizontal polarizations exhibited large fluctuations over the flight path (due to variable cloud cover), which prevented comparisons with the two-scale model, the figure shows that the third and fourth Stokes parameters remain relatively stable over the flight path for the three incidence angles and, agree quite well with

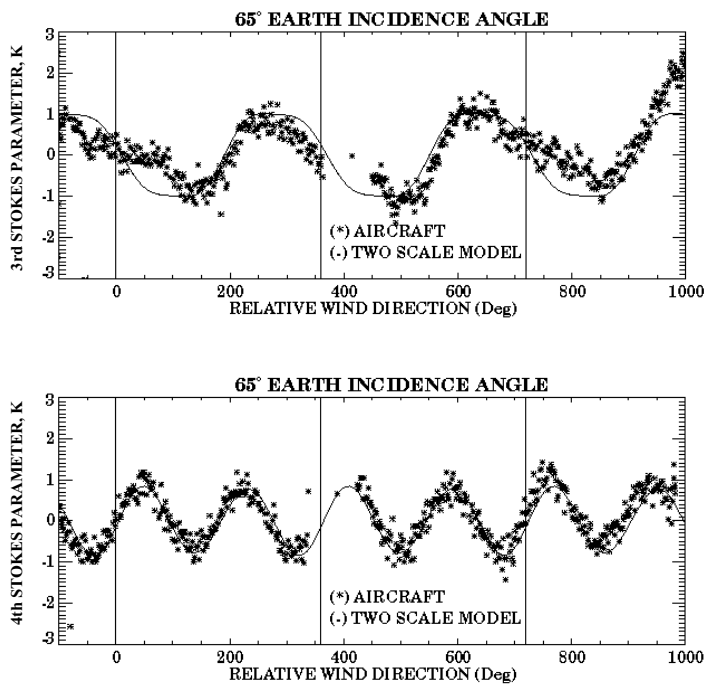

Figure 10. Comparisons of 10.7 GHz Aircraft Measurements (*) and DVY Model ($m = 0.75,\ R = 0.775;\ k_0/k_d = 5.0$) for $U_5 = 13\,\mathrm{m/s}$ and 65° Incidence Angle.

the two-scale model calculations. The heavy cloud conditions have not prevented accurate comparisons of the third and fourth Stokes parameters. Note the significant growth of the fourth Stokes parameter and the reduction of the second harmonic in the third Stokes parameter at the higher incidence angle.

6. SIMPLIFIED POLARIMETRIC MODEL

A first-order model of the polarimetric signatures may be constructed in terms of the azimuthal variability of the surface emissivity ε_a and the scattered sky brightness temperature incident on the surface T_a^r. (See (4) and (5) in [19]) That is, for a fixed incidence angle θ we may write

$$\begin{aligned} \varepsilon_a(\theta,\phi,U) &= \overline{\varepsilon}_a + \Delta\varepsilon_a(\theta,\phi,U) \\ T_a^r(\theta,\phi,U) &= \overline{T}_a^r + \Delta T_a^r(\theta,\phi,U) \end{aligned} \tag{14}$$

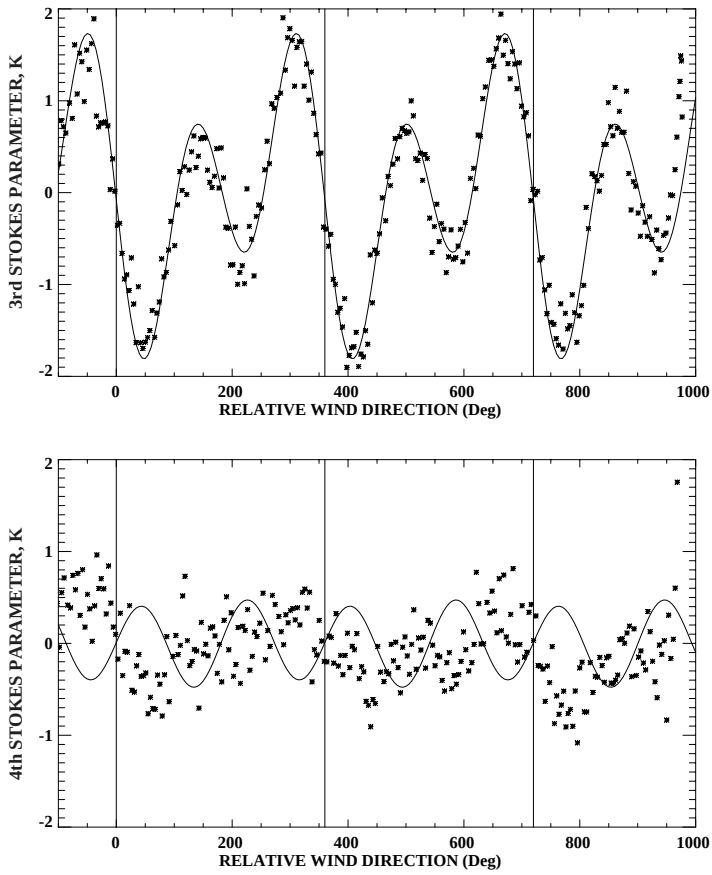

Figure 11. Comparisons of 10.7 GHz Aircraft Measurements (*) and DVY Model ($m = 0.75,\ R = 0.775;\ k_0/k_d = 5.0$) for $U_5 = 15\,\mathrm{m/s}$ and 45° Incidence Angle.

where a is the polarization of interest, φ is the azimuthal angle of observation relative to the up-wind direction and U is the surface windspeed which we reference to 19.5 m height. The bar denotes the azimuthal average. Furthermore, approximating ΔT_a^r with

$$\Delta T_a^r = \Delta R_a(\theta, \phi, U)\overline{T}_{sky}(\theta)$$

allows the polarimeter signals to be modeled in terms of $\Delta\varepsilon_a$ and ΔR_a. $\overline{T}_{sky}$ is the azimuthal average of the incident sky temperature. For the third and fourth Stokes parameters, aircraft observations and computations reported herein show that the azimuthal averages of the

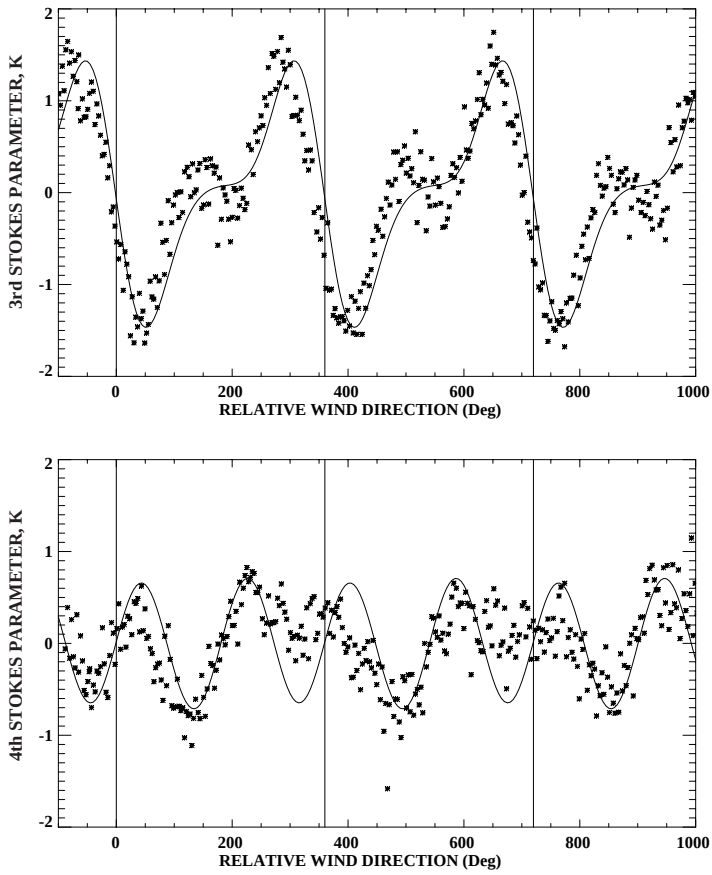

Figure 12. Comparisons of 10.7 GHz Aircraft Measurements (*) and DVY Model ($m = 0.75,\ R = 0.775;\ k_0/k_d = 5.0$) for $U_5 = 15\,\mathrm{m/s}$ and 55° Incidence Angle.

surface emissivity and scattered sky temperature vanish and hence will be omitted. Consequently, the polarimetric signatures upwelling from the ocean surface are then given by the quantity $\Delta\varepsilon_a\, T_{sea} + \Delta R_a\, T_{sky}$ with a denoting either vertical or horizontal polarizations or the third and fourth Stokes parameters.

To first-order we also neglect the small sea temperature and salinity dependencies of $\Delta\varepsilon_a$ and ΔR_a as well as harmonics of φ above the second. Approximating the coefficients of the first and second

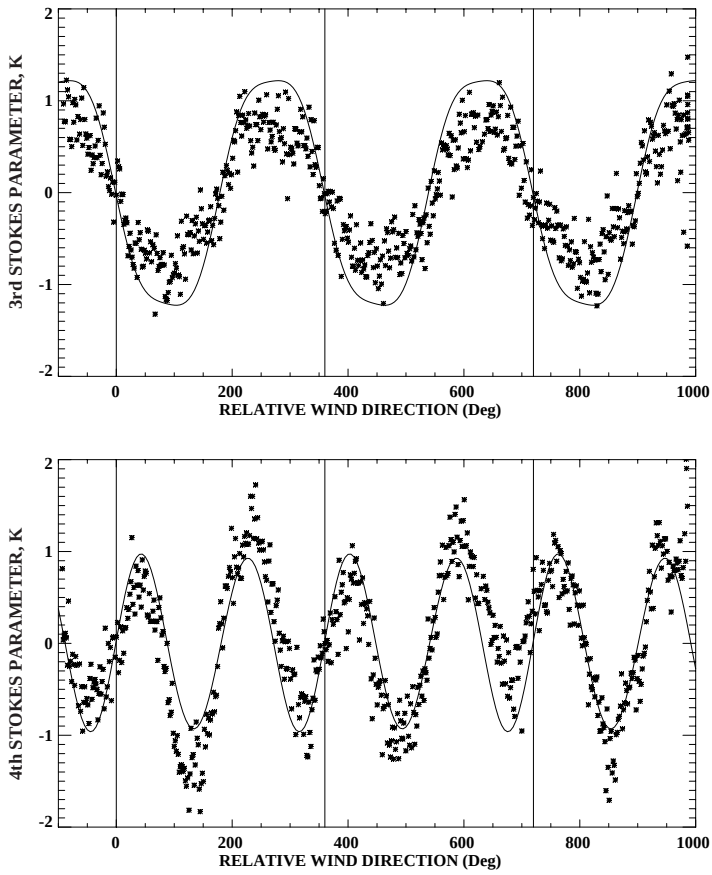

Figure 13. Comparisons of 10.7 GHz Aircraft Measurements (*) and DVY Model ($m = 0.75,\ R = 0.775;\ k_0/k_d = 5.0$) for $U_5 = 15\,\mathrm{m/s}$ and 65° Incidence Angle.

harmonics of φ with cubic polynomials of U we may write

$$\begin{aligned} \Delta\varepsilon_a &= A_1^{(a)} \cos\phi + A_2^{(a)} \cos 2\phi \\ \Delta R_a &= B_1^{(a)} \cos\phi + B_2^{(a)} \cos 2\phi \end{aligned} \tag{15}$$

where a identifies either the vertical or horizontal polarization and

$$\begin{aligned} A_i^{(a)} &= U\left(\alpha_{i1}^{(a)} + \alpha_{i2}^{(a)} U + \alpha_{i3}^{(a)} U^2\right) \quad i = 1, 2 \\ B_i^{(a)} &= U\left(\beta_{i1}^{(a)} + \beta_{i2}^{(a)} U + \beta_{i3}^{(a)} U^2\right) \quad i = 1, 2 \end{aligned} \tag{16}$$

Table 2. Coefficients of First-Order Polarimetric Model for 37 GHz and 53° Incidence Angle.

Polarization	Harmonic	$\Delta\varepsilon_a$			ΔR_a		
		$\alpha^{(a)}_{11}$	$\alpha^{(a)}_{12}$	$\alpha^{(a)}_{13}$	$\beta^{(a)}_{11}$	$\beta^{(a)}_{12}$	$\beta^{(a)}_{13}$
Vertical	cos ϕ	9.6367e-4	-8.6629e-5	3.5241e-6	9.5922e-4	-7.0580e-5	3.4287e-6
	cos 2ϕ	3.5253e-4	-5.2672e-5	2.0317e-6	-3.6055e-3	3.7708e-4	-1.1456e-5
Horizontal	cos ϕ	2.3005e-6	1.0002e-5	-1.3209e-7	2.0438e-3	-1.4944e-4	7.6005e-6
	cos 2ϕ	-1.4901e-3	1.4102e-4	-3.8482e-6	-1.5426e-3	1.5629e-4	-4.8888e-6
3rd Stokes	sin ϕ	-7.0647e-4	5.1532e-5	-2.2805e-6	-2.8868e-4	3.7524e-5	-5.9417e-7
	sin 2ϕ	-1.7890e-3	1.8547e-4	-5.5604e-6	3.4858e-3	-3.6125e-4	1.0727e-5
4th Stokes	sin ϕ	-7.4669e-5	7.4670e-6	-2.1485e-7	1.1665e-4	-1.0411e-5	2.5978e-7
	sin 2ϕ	5.3076e-4	-4.5194e-5	1.1187e-6	-7.0891e-4	6.0394e-5	-1.5117e-6

Table 3. Coefficients of First-Order Polarimetric Model for 19 GHz and 53° Incidence Angle.

Polarization	Harmonic	$\Delta\varepsilon_a$			ΔR_a		
		$\alpha^{(a)}_{11}$	$\alpha^{(a)}_{12}$	$\alpha^{(a)}_{13}$	$\beta^{(a)}_{11}$	$\beta^{(a)}_{12}$	$\beta^{(a)}_{13}$
Vertical	cos ϕ	1.0462e-3	-1.0482e-4	4.2781e-6	1.2638e-3	-9.2418e-5	4.2095e-6
	cos 2ϕ	1.7721e-4	-2.8289e-5	1.1142e-6	-3.6313e-3	4.0482e-4	-1.2888e-5
Horizontal	cos ϕ	8.5178e-5	-2.7159e-6	5.3669e-7	1.8283e-3	-1.4126e-4	6.4939e-6
	cos 2ϕ	-1.6235e-3	1.7160e-4	-5.2641e-6	-2.8091e-3	3.3690e-4	-1.1361e-5
3rd Stokes	sin ϕ	-6.2687e-4	5.2948e-5	-2.0692e-6	-4.0810e-4	4.2275e-5	-1.1897e-6
	sin 2ϕ	-1.8096e-3	1.9882e-4	-6.3008e-6	2.1905e-3	-2.3179e-4	7.0958e-6
4th Stokes	sin ϕ	-8.2037e-5	8.6260e-6	-2.6006e-7	1.4312e-4	-1.3322e-5	3.5015e-7
	sin 2ϕ	8.1354e-4	-7.9704e-5	2.2798e-6	-9.7199e-4	9.1230e-5	-2.5189e-6

The third and fourth Stokes brightness temperatures is modeled by

$$\begin{aligned} \Delta\varepsilon_a &= A_1^{(a)} \sin\phi + A_2^{(a)} \sin 2\phi \\ \Delta R_a &= B_1^{(a)} \sin\phi + B_2^{(a)} \sin 2\phi \end{aligned} \tag{17}$$

with expressions similar to (16) for $A_i^{(a)}$ and $B_i^{(a)}$. Tables 2 through 5 present the coefficients for an incidence angle of 53° for 37, 19.35, 10.7 and 6.8 GHz. The coefficients are presented in scientific notation.

Table 4. Coefficients of First-Order Polarimetric Model for 10.7 GHz and 53° Incidence Angle.

Polarization	Harmonic	$\Delta\varepsilon_a$			ΔR_a		
		$\alpha^{(a)}_{11}$	$\alpha^{(a)}_{12}$	$\alpha^{(a)}_{13}$	$\beta^{(a)}_{11}$	$\beta^{(a)}_{12}$	$\beta^{(a)}_{13}$
Vertical	**cos ϕ**	8.8842e-4	-9.0366e-5	3.6308e-6	1.4755e-3	-1.1260e-4	5.0382e-6
	cos 2ϕ	-1.1292e-4	1.5072e-5	-5.8729e-7	-2.5219e-3	2.9104e-4	-9.4800e-6
Horizontal	**cos ϕ**	9.3039e-5	-4.6807e-6	5.2923e-7	1.4272e-3	-1.0902e-4	5.0144e-6
	cos 2ϕ	-1.4274e-3	1.6772e-4	-5.6149e-6	-2.5480e-3	3.1332e-4	-1.0652e-5
3rd Stokes	**sin ϕ**	-4.6950e-4	4.3699e-5	-1.6267e-6	-4.8487e-4	3.9792e-5	-1.2953e-6
	sin 2ϕ	-1.2050e-3	1.3263e-4	-4.1836e-6	6.6633e-4	-6.4229e-5	1.8349e-6
4th Stokes	**sin ϕ**	-6.5443e-5	6.9366e-6	-2.1015e-7	1.3404e-4	-1.2231e-5	3.1955e-7
	sin 2ϕ	8.6168e-4	-9.0416e-5	2.7454e-6	-9.7466e-4	9.5753e-5	-2.7626e-6

Table 5. Coefficients of First-Order Polarimetric Model for 6.8 GHz and 53° Incidence Angle.

Polarization	Harmonic	$\Delta\varepsilon_a$			ΔR_a		
		$\alpha^{(a)}_{11}$	$\alpha^{(a)}_{12}$	$\alpha^{(a)}_{13}$	$\beta^{(a)}_{11}$	$\beta^{(a)}_{12}$	$\beta^{(a)}_{13}$
Vertical	**cos ϕ**	4.7592e-4	-4.1933e-5	1.7062e-6	1.4253e-3	-1.1444e-4	4.9676e-6
	cos 2ϕ	-1.4941e-4	2.0848e-5	-7.7670e-7	-1.4356e-3	1.7286e-4	-5.8191e-6
Horizontal	**cos ϕ**	8.8925e-5	-4.5038e-6	4.2915e-6	1.1047e-3	-8.4853e-5	3.8606e-6
	cos 2ϕ	-1.0042e-3	1.2019e-4	-4.0317e-6	-1.6349e-3	2.0933e-4	-7.3307e-6
3rd Stokes	**sin ϕ**	-3.2320e-4	2.9299e-5	-1.0298e-6	-4.8349e-4	4.0686e-5	-1.4441e-6
	sin 2ϕ	-9.6928e-4	1.0810e-4	-3.4336e-6	1.8759e-4	-1.3405e-5	2.7263e-7
4th Stokes	**sin ϕ**	-5.5539e-5	5.9531e-6	-1.8147e-7	1.1571e-4	-1.0632e-5	2.8094e-7
	sin 2ϕ	7.7916e-4	-8.4307e-5	2.6227e-6	-8.5648e-4	8.6418e-5	-2.5496e-6

7. CONCLUSIONS

We have shown that the two-scale scattering and emission theory in concert with the Durden/Vesecky/Yueh elevation spectral model and an ad hoc set of parameters provides an accurate model of microwave Stokes parameters of the sea. Essentially all of the azimuthal features, amplitude and phase, appearing in aircraft polarimetric measurements at 10.7, 19.35 and 37 GHz and SSM/I vertical and horizontal signals at 19.35 and 37 GHz have been "explained" on the basis of this model, providing validation of the two scale scattering theory developed in [19] for the range of conditions considered. Issues requiring further

research include (1) the windspeed dependence of the spectral model parameters, i.e., the hydrodynamic modulation m and ratio R of cross-wind to up-wind slope variances of the complete elevation spectra and (2) a better understanding of the wind direction signal at low wind speeds. In addition, a more physically-based elevation model needs investigation to provide understanding of the hydrodynamic modulation process contained in the empirical parameter set reported herein. The effects of sea foam, fetch and atmospheric instability must also be incorporated to obtain a complete ocean polarimetry emission model. In spite of these issues, the two-scale scattering model should be useful in studies concerned with the retrieval of surface wind direction from satellite polarimetric measurements.

ACKNOWLEDGMENT

We wish to thank Dr. S. Yueh for providing the 19.35 and 37 GHz aircraft data and Mr. A. Uliana for computer programming support and assistance with preparation of the figures. We also acknowledge valuable conversations with Dr. Alex Stogryn on the modeling of the ocean surface. Finally, we gratefully acknowledge Dr. Stephen Mango of the Integrated Program Office of the National Polar-Orbiting Operational Environmental Satellite System and Dr. Michael VanWoert, formerly of the Office of Naval Research, for their long standing support of this work.

REFERENCES

1. Durden, S. L. and J. F. Vesecky, "A physical radar cross-section model for a wind-driven sea with swell," *J. Ocean Engr.,* Vol. OE-10, No. 4, 445–451, 1985.
2. Yueh, S. H., "Modeling of wind direction signals in polarimetric sea surface brightness temperatures," *IEEE Trans. Geosci. Remote Sensing,* Vol. 35, No. 6, 1400–1418, 1997.
3. Yueh, S. H., W. J. Wilson, F. K. Li, W. B. Ricketts, and S. V. Nghiem, "Polarimetric brightness temperatures of sea surfaces measured with aircraft K- and Ka-band radiometers," *IEEE Trans. Geosci. Remote Sensing,* Vol. 33, No. 5, 1177–1187, 1997.
4. Chang, P. S., P. W. Gaiser, L. Li, and K. M. St. Germain, "Multi-frequency polarimetric microwave ocean wind direction retrievals," *Proceedings of the International Geoscience and Remote Sensing Symposium, 1997,* Singapore, 1997.

5. Yueh, S. H., W. J. Wilson, S. J. DiNardo, and F. K. Li, "Polarimetric microwave brightness signatures of ocean wind direction," *IEEE Trans. Geosci. Remote Sensing,* Vol. 37, No. 2, 949–959, 1999.
6. Wentz, F. J., "Measurement of oceanic wind vector using satellite microwave radiometers," *IEEE Trans. Geosci. Remote Sensing,* Vol. 30, No. 5, 960–972, 1992.
7. Meissner, T. and F. J. Wentz, "An updated analysis of the ocean surface wind direction signal in passive microwave brightness temperatures," submitted to *IEEE Trans. Geosci. Remote Sensing,* 2002.
8. Chang, P. S. and L. Li, "Ocean surface wind speed and direction retrievals from the SSM/I," *IEEE Trans. Geosci. Remote Sensing,* Vol. 36, No. 6, 1866–1871, 1998.
9. Wick, G. A., J. J. Bates, and C. C. Gottschall, "Observational evidence of a wind direction signal in SSM/I passive microwave data," *IEEE Trans. Geosci. Remote Sensing,* Vol. 38, No. 2, 823–837, 2000.
10. Piepmeier, J. R. and A. J. Gasiewski, "High-resolution passive polarimetric microwave mapping of the ocean surface wind vector fields," *IEEE Trans. Geosci. Remote Sensing,* Vol. 39, No. 3, 606–622, 2001.
11. Hollinger, J. P., "Passive microwave measurements of sea surface roughness," *IEEE Trans. Geoscience Elect.,* Vol. GE-9, No. 3, 165–169, 1971.
12. Stogryn, A. P., "The apparent temperature of the sea at microwave frequencies," *IEEE Trans. Ant. Prop.,* Vol. AP-15, No. 2, 278–286, 1967.
13. Cox, C. S. and W. H. Munk, "Measurements of the roughness of the sea surface from photographs of the sun's glitter," *J. Opt. Soc. Am.,* Vol. 44, 838–850, 1954.
14. Hollinger, J. P., "Passive microwave measurements of the sea surface," *J. Geophys. Res.,* Vol. 75, No. 27, 5209–5213, 1970.
15. Semyonov, B. I., "Approximate computation of scattering of electromagnetic waves by rough surface contours," *Radio Eng. Electron Phys.,* Vol. 11, 1179–1187, 1966.
16. Wu, S. T. and A. K. Fung, "A non-coherent model for microwave emissions and backscattering from the sea surface," *J. Geophys. Res.,* Vol. 77, No. 30, 5917–5929, 1972.
17. Wentz, F. J., "A two-scale scattering model for foam-free sea microwave brightness temperatures," *J. Geophys. Res.,* Vol. 80,

No. 24, 3441–3446, 1975.

18. Yueh, S. H., et al., "Polarimetric passive remote sensing of ocean wind vectors," *Radio Sci.,* Vol. 29, No. 4, 799–814, 1994.
19. Poe, G. A., K. M. St. Germain, and P. W. Gaiser, "Theory of polarimetric emission model of the sea at microwave frequencies," Naval Research Laboratory Technical Memorandum Report, in press, 2002.
20. Stogryn, A. P., "A study of radiometric emission from a rough sea surface," NASA Report CR-2088, Contract 1-10633, 1972.
21. Durden, S. L. and J. F. Vesecky, "A numerical study of the separation wavenumber in the two-scale scattering approximation," *IEEE Trans. Geosci. Remote Sensing,* Vol. 28, No. 2, 271–272, 1990.
22. Fung, A. K. and K. K. Lee, "A semi-empirical sea-spectrum model for scattering coefficient estimation," *IEEE Ocean Engr.,* Vol. OE-7, No. 4, 166–176, 1982.
23. Donelan, M. A. and W. J. Pierson, Jr., "Radar scattering and equilibrium ranges and wind-generated waves with application to scatterometry," *J. Geophys. Res.,* Vol. 92, No. C5, 4971–5029, 1987.
24. Stogryn, A. P., "Equations for the permittivity of sea water," Report to Naval Research Laboratory, Washington, D.C., Code 7223, Aug. 1997.
25. Yueh, S. H., W. J. Wilson, F. K. Li, W. B. Ricketts, and S. V. Nghiem, "Polarimetric measurements of sea surface brightness temperatures using an aircraft K-band radiometer," *IEEE Trans. Geosci. Remote Sensing,* Vol. 33, No. 1, 85–92, 1995.
26. Kunkee, D. B. and A. J. Gasiewski, "Simulation of passive microwave wind direction signatures over the ocean using an asymmetrices wave geometrical optics model," *Radio Science,* Vol. 32, No. 1, 59–78, Jan. 1997.